GIScience & Remote Sensing

Estimating upper soil horizon carbon stocks in a permafrost watershed of Northeast Siberia by integrating field measurements with Landsat-5 TM and WorldView-2 satellite data

Dylan E. Broderick[a], Karen E. Frey[a], John Rogan[a], Heather D. Alexander[b] & Nikita S. Zimov[c]

[a] Graduate School of Geography, Clark University, 950 Main St., Worcester, MA 01610, USA

[b] Department of Biological Sciences, University of Texas at Brownsville, 80 Fort Brown, Brownsville, TX 78520, USA

[c] Northeast Science Station, Pacific Institute of Geography, Far East Branch of the Russian Academy of Sciences, Cherskiy, Republic of Sakha (Yakutia), Russian Federation
Published online: 05 Mar 2015.

PLEASE SCROLL DOWN FOR ARTICLE

Taylor & Francis
Taylor & Francis Group

Estimating upper soil horizon carbon stocks in a permafrost watershed of Northeast Siberia by integrating field measurements with Landsat-5 TM and WorldView-2 satellite data

Dylan E. Broderick[a]*, Karen E. Frey[a], John Rogan[a], Heather D. Alexander[b] and Nikita S. Zimov[c]

*[a]Graduate School of Geography, Clark University, 950 Main St., Worcester, MA 01610, USA;
[b]Department of Biological Sciences, University of Texas at Brownsville, 80 Fort Brown, Brownsville, TX 78520, USA; [c]Northeast Science Station, Pacific Institute of Geography, Far East Branch of the Russian Academy of Sciences, Cherskiy, Republic of Sakha (Yakutia), Russian Federation*

Arctic soils contain three times as much carbon (C) as all aboveground biomass distributed globally, much of which is stored in permafrost soils. Here, we (1) determine the predictability of estimating soil organic carbon (SOC) using different satellite data, classifications, and methods; (2) estimate the quantity and distribution of SOC for the top 10 cm for the Ambolikha River watershed (~121 km^2) in northeast Siberia, a sub-watershed of the Kolyma River; and (3) produce a hybrid SOC map through data fusion, combining the strengths of each data type. Land cover maps were produced using a pixel-based classification with Landsat-5 Thematic Mapper (TM) data and an object-based classification using WorldView-2 data. Spectral mixture analysis (SMA) was performed on both data types to calculate the fraction of four vegetation types in each pixel, and land cover maps were combined with field measurements of SOC in the top 10 cm. The overall classification accuracy was 69% for Landsat, 81% for WorldView-2, and 82% for the hybrid map. The hybrid map estimated 490.5 Gg of SOC for the top 10 cm within the Ambolikha River watershed, with less severe over- or under-estimated than the Landsat or WorldView-2 maps alone. The results suggest that (a) higher spatial resolution satellite data and object-based classification should be used for land cover classification in the Arctic; (b) integrating multiple sensors maximizes the strengths of different sensors for estimating SOC; and (c) previous studies performed at the regional or pan-Arctic scale using lower spatial resolution data likely underestimate total SOC.

Keywords: Arctic; Kolyma River; soil carbon; WorldView-2; Landsat-5 TM; hybrid map; belowground carbon

1. Introduction

Northern high latitudes are experiencing climate change effects earlier and more severely than other regions of the globe, particularly with regard to carbon (C) fluxes between aquatic, terrestrial, and atmospheric pools (Grosse et al. 2011). In the Arctic, the largest pool of terrestrial organic C is stored in soils, which contain approximately three times the amount of C stored in global terrestrial aboveground biomass (Jobbágy and Jackson 2000; Schuur et al. 2008). The northern permafrost (i.e., perennially frozen ground) region is approximately 18.8 million km^2 in size and includes 16% of global soil area (Hugelius

---

*Corresponding author. Email: dbroderick@clarku.edu

et al. 2010). Increased warming and associated permafrost thaw are causing large amounts of SOC to decompose quickly and subsequently be released to the atmosphere as CO_2 and methane (Zimov et al. 2006). Anisimov, Nelson, and Pavlov (1999) predicted that up to 25% of SOC stored in northern peatlands and permafrost has the potential to flux to the atmosphere during the twenty-first century owing to enhanced warming, equivalent to approximately 100 Pg C (or an additional 47 ppm of C to the global atmosphere). This release of C as greenhouse gas is potentially large enough to increase local and global surface temperatures by up to 4°C, further operating as positive feedback on climate warming (Oechel and Vourlitis 1994). Monitoring C dynamics and estimating regional belowground C stores, along with associated impacts on aboveground vegetation and wetlands, can therefore be instructive in predicting the rate and intensity of future warming trends (Schuur et al. 2008; Potter 2014).

Northern Siberia comprises the majority of Arctic land areas and is therefore an important region for studying the impacts of climate warming on SOC at northern high latitudes (Tarnocai et al. 2009). The Kolyma River in northeastern Siberia, among the largest rivers draining to the Arctic Ocean, is particularly important because it is the largest Arctic river basin completely underlain by continuous permafrost (Zimov et al. 2006). C-rich so-called yedoma soils (i.e., Pleistocene-aged loess deposits containing 50–90% ice) of this watershed contain up to 500 Pg C, with continuous permafrost reaching up to 650 m in depth (Kajimoto et al. 2006; Walter et al. 2006; Schuur et al. 2008). Approximately 88% of C in northern permafrost regions is found below-ground, yet this C pool is also one of the least studied (Hugelius et al. 2010). Several recent studies have estimated aboveground biomass and C content within the lower Kolyma River basin (Kajimoto et al. 2006; Alexander et al. 2012; Berner et al. 2012), yet none to date have utilized satellite data to estimate belowground C specifically. Owing to accessibility limitations in remote regions of the Arctic, it is often difficult to estimate C across large, diverse landscapes using field data alone (Fuchs et al. 2009).

Satellite remote sensing provides the capability to produce spatially continuous estimates of belowground C at the landscape scale (Heikkinen et al. 2004; Szakacs et al. 2011). Although remotely sensed data cannot directly measure specific components of the C cycle, they are commonly used to observe biophysical phenomena related to C storage and flux (Sitch et al. 2007). In particular, relating SOC quantities with the land cover type is a newly emerging method for linking ground measurements to remotely sensed data (Sitch et al. 2007; Zhou et al. 2008; Szakacs et al. 2011). SOC storage and decomposition are strongly influenced by vegetation dynamics, which in turn are largely controlled by hydrology, temperature, disturbance regime, and soil biogeochemical conditions (Grosse et al. 2011). The vegetation type and land cover can be mapped successfully using several different classification methods, often determined by the spatial and spectral resolutions of the available data (Turner, Ollinger, and Kimball 2004). Pixel-based classifiers such as maximum likelihood (Max Like) are commonly used for medium (i.e., spatial resolution 5–250 m) and coarse (i.e., spatial resolution >250 m) data, where each pixel is classified based on its spectral properties (Rogan and Chen 2004; Perea, Meroño, and Aguilera 2009; Zhang and Zhu 2011). At fine spatial resolutions (i.e., <5 m), however, object-based classification is often employed to create exclusive segments of pixels with similar spectral, texture, and shape characteristics (Zhang and Zhu 2011).

A variety of studies related to satellite data types have compared the use of fine and medium spatial resolution data and image classification methods, often supporting the use of fine resolution imagery in highly heterogeneous landscapes in both urban (Thomas, Hendrix, and Congalton 2003; Giner and Rogan 2012; Tang and Pannelli 2009) and

vegetated locations (Stow et al. 2004; Wulder et al. 2004; Fuchs et al. 2009; Huang et al. 2009). Although many previous studies relate the land cover classification maps to C stocks (Wulder et al. 2004; Fuchs et al. 2009), most are concerned with aboveground biomass alone owing to a stronger correlation with biophysical characteristics that can be measured remotely (Turner, Ollinger, and Kimball 2004; Fuchs et al. 2009; Berner et al. 2012). Until now, no studies have produced estimates of belowground SOC storage in the Arctic using multiple spatial resolution data or compared the quantitative differences that may result. Additionally, no studies have used data of different spatial resolutions to develop a hybrid land cover classification map and further estimate associated SOC quantities across a landscape. Given the estimates of large SOC stocks in permafrost landscapes, it is necessary to explore different data types and methods used to quantify these C reservoirs in order to establish effective practices for future studies in the region.

The objectives of this study were to (1) determine the predictability of estimating soil organic carbon (SOC) using different satellite data, classifications, and methods; (2) estimate the quantity and distribution of SOC for the top 10 cm for the Ambolikha River watershed (~121 km^2) in northeast Siberia, a sub-watershed of the Kolyma River; and (3) produce a hybrid SOC map through data fusion, combining the strengths of each data type. Medium spatial resolution data from Landsat-5 Thematic Mapper (TM) and fine spatial resolution data from WorldView-2 were used to produce two land cover maps, using a Max Like algorithm and an object-based segmentation algorithm, respectively. The resulting maps were compared to determine the most appropriate available data type and the method for SOC mapping in this region. The classes that were most accurately mapped by each sensor were then combined in a hybrid map through data fusion to produce the best estimate of total SOC. Here, we introduce a satellite-based quantification of belowground C stores, providing an assessment of a set of methods for such investigations. Furthermore, the findings of this research will be useful to help streamline large-area studies of SOC in support of field monitoring efforts, which is particularly critical for regions such as the Kolyma River basin that may be highly susceptible to C release through climate warming.

2. Study area

The Ambolikha River watershed (approximately 68.459–68.737°N, 161.313–161.459°E) is an area of ~121 km^2 located in northeastern Siberia, located 240 km north of the Arctic Circle near the city of Cherskiy (Figure 1). The area belongs to the administrative region of Sakha Republic (formerly Yakutia) of the Russian Federation and is a sub-watershed of the Kolyma River. Though this study deals primarily with terrestrial SOC, we chose a watershed delineation to facilitate linking results to past and future studies for the area concerned with aquatic and atmospheric C reservoirs. In particular, an increasing number of studies have taken a watershed approach to understanding C storage and flux across the Arctic landscape (e.g., Frey and Smith 2005; Tank et al. 2012; Denfeld et al. 2013). Topography of the Ambolikha watershed is generally flat, with elevation ranging from 3 to 40 m above the sea level. Owing to the shallow relief, the watershed is also comprised of numerous small rivers, streams, and lakes with diameters ranging from 5 to >2000 m. Many of these so-called thermokarst lakes formed as thawing permafrost created depressions in the landscape that were then filled with surface water. Drained lake basins, or alases, may also form as these lakes terrestrialize with peat and subsequently dry up (Koutaniemi 1985). The region is underlain with ~350–650 m deep continuous permafrost, with an active layer (the upper layer of soil that thaws and refreezes seasonally)
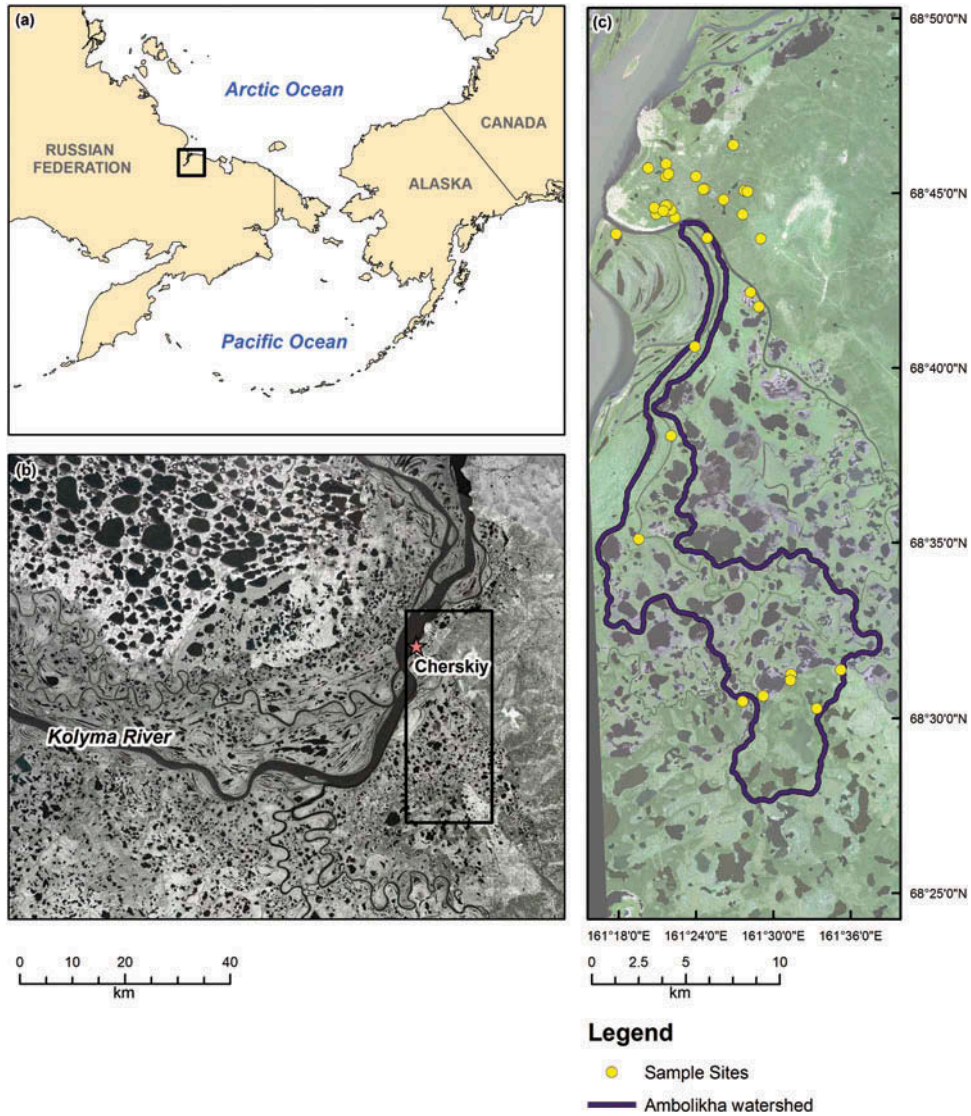
Figure 1.   (a) Study area showing the location of the Ambolikha River watershed in Northeast Siberia, with (b) a panchromatic image from Landsat-5 TM (30 m spatial resolution) captured on 11 July 2011 and (c) a WorldView-2 (1.85 m spatial resolution) true color composite (RGB = 5, 3, 2) captured on 12 July 2011 ((b) is outlined in (a), (c) is outlined in (b)).

depth ranging from 0 cm in February to 20–50 cm in July (Walter et al. 2006; Schuur et al. 2008). The climate is cold and continental, with average temperatures ranging from ~−35°C in January to ~18°C in July, and the average total annual precipitation ranging from ~200–215 mm (Corradi et al. 2005; NCDC 2012). While the length and size of the Kolyma River basin (approximately 2130 km and 664,000 km^2, respectively) result in larger variations in topography, vegetation, and climate across its geographic extent, the vegetation, soil, topography, and hydrology of the Ambolikha watershed are representative of Arctic lowland regions of the Kolyma River basin.

Although there is relatively low diversity in terms of tree and shrub species, the land cover and tree stand density are highly heterogeneous at the landscape scale. The deciduous needle-leaf species *Larix cajanderi* (Cajander larch) is the dominant tree type of the region. Other vegetation types consist largely of shrub and understory species including *Betula divaricate* and *Betula exilis* (dwarf birch); *Pinus pumila* (dwarf pine); *Ledum decumbens* (Labrador tea); *Salix pulchra, Salix alaxensis,* and *Salix glauca* (dwarf willow); and a variety of mosses and grasses (Kajimoto et al. 2006; Abaimov 2010). Dominant soil types include entisols, gelisols, and loess deposits, which comprise Pleistocene-aged yedoma soils. The fire regime for the region is linked to both summer temperatures and aboveground biomass, and has a return interval of 50–120 years (Furyaev et al. 2001; Schepaschenko, Shvidenko, and Shalaev 2008).

3.   Data and methods

3.1.   *Satellite and ancillary data*

A 30 m Landsat-5 Thematic Mapper (TM) image (optical bands 1–5 and 7; 8-bit radiometric resolution) captured on 11 July 2011 (path 105, row 12) was used to map land cover in the Ambolikha watershed (see Table 1 for wavelength designations). The image was 100% cloud-free and corresponded with the time of year when field measurements were collected (i.e., July 2010, 2011, and 2012). Atmospheric correction was performed using the cos(T) model, which subtracts non-zero pixel values for dark objects from all other pixels in the image to remove haze effects and converts digital numbers (DNs) to surface reflectance (Chavez 1996). The images were left in their original Universal Transverse Mercator (UTM) projection (zone 57 N), as it was received from the US Geological Survey.

Panchromatic and multispectral WorldView-2 (bands 2, 3, 5, and 7; 11-bit radiometric resolution) data captured on 12 July 2011 with spatial resolutions of 0.46 m (panchromatic) and 1.85 m (multispectral) were used to map land cover across the watershed (see Table 1 for wavelength designations). The images were radiometrically corrected using dark object subtraction to account for variability in detector response and differences in gain and offset that may result in a non-uniform image (Updike and Comp 2010). Additional atmospheric correction (e.g., conversion to top-of-atmosphere spectral radiance) was unnecessary because all WorldView-2 images were collected on the same day and all pixel values were therefore relative to one another. Images were converted from their original north polar stereographic projection to a UTM projection

Table 1.   Bands and wavelength ranges (in micrometers) for the Landsat-5 and WorldView-2 bands utilized for land cover classification.

Landsat-5 TM		WorldView-2	
Band	Wavelength (μm)	Band	Wavelength (μm)
1 (Blue)	0.45–0.52	Panchromatic	0.45–0.81
2 (Green)	0.52–0.60	2 (blue)	0.42–0.52
3 (Red)	0.63–0.69	3 (green)	0.51–0.59
4 (Near-infrared)	0.76–0.90	5 (red)	0.62–0.69
5 (Short-wave infrared)	1.55–1.75	7 (near-infrared1)	0.77–0.90
7 (Short-wave infrared)	2.08–2.35		

(zone 57 N) for consistency with the Landsat-5 image. An independent set of validation sites (150 per land cover class; support size 1 m^2) was also selected randomly using the WorldView-2 image to assess the accuracy of the Landsat-5 and WorldView-2 land cover classifications.

Ancillary data include a northern circumpolar soil map with a minimum mapping unit of 10 km^2 from the National Snow and Ice Data Center (NSIDC; Tarnocai et al. 2002); a northern Eurasia land cover map with 29 categories and a 1 km spatial resolution from Global Land Cover 2000 (GEM; Bartalev et al. 2003); and the digital elevation model and stream layers from the USGS Hydro 1 K dataset for Asia, both with a 1 km spatial resolution (USGS 2011).

3.2.   *Field data collection*

SOC was estimated at 35 terrestrial sites in July 2010, 2011, and 2012 (Figure 1). Though 26 sites fell slightly outside of the study area boundary (within 0.5–4.5 km), they are still closely representative of the vegetation conditions in the watershed, increase the robustness of sites per land cover class, and are used in this study as a test case for larger scale analyses. Sites were categorized as larch forest, shrub (<50% larch), floodplain (low-lying areas seasonally inundated with melt water from lakes and streams), or alas (Figure 2). Sites were selected to be representative of each cover type, and subsequently consisted of varying stand densities and ages, species composition, and topography in order to encompass their variability. At least three soil cores extending to 10 cm were extracted at each site. While the majority of cores were comprised entirely of organic materials, cores at several sites also included mineral soil as the organic layer was shallower than 10 cm. Field measurements included the organic layer depth (within the active layer), mineral soil depth (if applicable), thaw depth, humic layer depth, and dimensions of the core for each sample. Samples collected at five lakes in 2012 using a hand-held Van Veen Grab were also incorporated to estimate C content of lake-bottom sediments.

To estimate C content, soil and sediment samples from each site were weighed and combined with volume measurements to calculate bulk density (the product of the dry soil weight and core volume). Samples were then homogenized, subsampled, weighed, and dried for 48 hours at 60°C. Next, samples were weighed again and placed in a muffle furnace for 4 hours at 450° C to measure loss on ignition (LOI). The difference in weight before and after combustion was assumed to be the organic content of the sample (modified from Reeuwijk 2002). Percent C for each sample was determined using the following formula for C content (e.g., Alexander et al. 2012):

$$C \text{ content} = 0.51^*LOI - 0.6. \tag{1}$$

Soil C was estimated in terms of grams per square meter (g C m^{-2}) by multiplying percent C, bulk density, and depth measurements for each core. Average organic layer depths (within the thawed active layer) and standard errors (SE) for each land cover type were determined based on field measurements, and the average soil C content by site and by land cover type was calculated for the top 10 cm of the soil column. We provided estimates for the top 10 cm to be comparable with findings from other studies (e.g., Hugelius et al. 2013) and to calculate SOC consistently across the watershed regardless of the topography or land cover type.
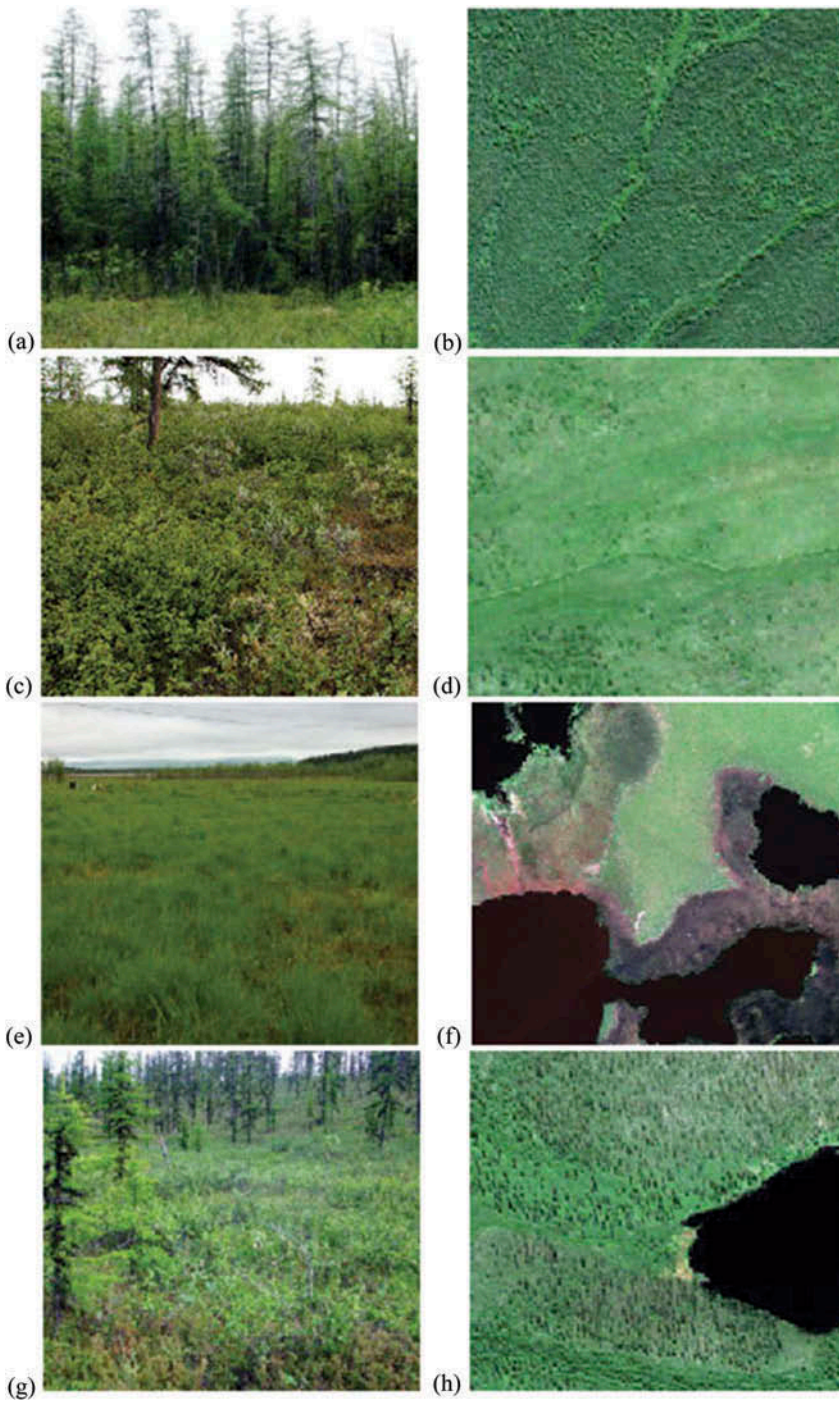
Figure 2. Ground photographs of (a) larch, (c) shrub, (e) floodplain, and (g) alas vegetation types used in field sampling and land-cover classification with respective aerial examples (b), (d), (f), and (h) from a WorldView-2 (1.85 m spatial resolution) true color composite (RGB = 5, 3, 2) captured on 12 July 2011.

3.3. *Land cover classification*

Image analysis was performed using the IDRISI Selva image-processing software (Eastman 2012a). The first land cover classification effort utilized the Landsat-5 data and pixel-based Max Like algorithm. Max Like is a parametric classifier that assumes a normal distribution of statistics for each class defined based on calibration data, and assigns pixels to the class with the highest probability according to a covariance matrix and mean vector (Richards 1986; Shafri, Suhaili, and Mansor 2007). Calibration sites for bare soil, water, larch forest, shrub, floodplain, and alas were defined across the Ambolikha watershed. Relative probabilities of the expected frequency of each cover type were assigned to guide the classification, which was based on Landsat bands 1–5 and 7 (see Table 1), using ancillary data and knowledge of the study area. Lakes were manually delineated within the water category, and the hard-classified map was reclassified to isolate the lakes and the four vegetation classes (larch forest, shrub, floodplain, and alas).

Linear spectral mixture analysis (SMA) was performed on the spectral reflectance data by manually selecting pure taxonomic image endmembers as training sites for each of the four vegetation classes to produce fraction images. These fraction images estimated the percentage of each vegetation type contained in each pixel (e.g., Settle and Drake 1993). A residual image, which displayed the degree to which a pixel's composition could not be attributed to one of the defined taxonomic endmembers, was produced using the following formula:

$$\varepsilon_i = b_i \sum_{i-1}^{n} \left(a_{ij} x_j \right) \tag{2}$$

where b is the spectral reflectance for the ith band of the pixel, a is the spectral reflectance of the jth component in the pixel for the ith spectral band, i is the number of spectral bands, j is the number of components in the mixture, and x is the fraction value of the jth component in the pixel (Sohn and McCoy 1997). The residual image was used to determine which locations were not easily designated as a specific mixture of vegetation types, and SMA was rerun with additional training sites until the root mean square error (RMSE) was less than 0.1.

The second land cover classification involved WorldView-2 imagery and an object-based segmentation algorithm using WorldView-2 bands 2, 3, 5, and 7 (see Table 1). Pixels were first grouped into segments based on similar spectral, texture, and shape properties using the segmentation module in IDRISI Selva (Eastman 2012a). A surface image of the variance within each pixel, based on a 3×3 moving window and the four equally weighted bands, was produced to group pixels within a homogeneous region had low values. Similar to a watershed delineation process, pixels were grouped if they were in the same catchment, and segments were then created. The process worked iteratively to compare segments with their neighbors, considering both the surface image and spectral characteristics of adjacent segments using the formula:

$$\text{Diff} = \sum_{i=1}^{n} \text{Weight}_i \times \left(\text{Weight}_{\text{mean}} \times \text{DiffMean}_i + \text{Weight}_{\text{Std}_{\text{dev}}} \times \text{DiffStd}_{\text{Dev}i} \right) \tag{3}$$

Where Diff is the overall heterogeneity for a given segment; n is the number of input images; Weight_i, $\text{Weight}_{\text{mean}}$, and $\text{Weight}_{\text{Std\_dev}}$ are equally weighted input parameters;

DiffMean$_i$ is the standardized difference in mean and standard deviations for the spectral reflectance of all pixels in a potential segment; and DiffStd_Dev$_i$ is the range of differences of standard deviations between two segments (Eastman 2012b). Calibration sites for the above six land cover categories were defined on a segment-by-segment basis across the Ambolikha watershed. The Segclass module was used to create the object-based classification by combining calibration sites, the pixel-based Max Like classification, and the segment image. Rather than assigning individual pixels to a class, classification was determined by the majority class within a segment (Eastman 2012b). As with the Landsat-5 classification, the image was reclassified to include only lakes and vegetation classes (larch forest, shrub, floodplain, and alas). SMA was then performed using the four vegetation classes and taxonomic image endmembers for the segmentation classification to produce fraction images for each vegetation type.

To compare the agreement between the Landsat-5 and WorldView-2 classifications directly, the 30 m Landsat-5 map was upsampled to match the pixel size of the WorldView-2 map. A cross-tabulation matrix was generated between these two maps showing agreement and disagreement overall and by land cover type. An independent set of validation sites (150 per class) was derived using stratified random sampling and the panchromatic WorldView-2 image to assess the accuracy of the Landsat-5 and WorldView-2 classifications and to determine which data type produced more reliable results. Values were recorded in a confusion matrix, where the overall accuracy was calculated as the sum of the diagonal values over the total number of randomly sampled pixels (Gupta et al. 2004).

3.4. Soil C estimation

Soil C maps for the top 10 cm were created for the Ambolikha watershed using the field data of average SOC values by the land cover type and the SMA outputs based on the Landsat-5 and WorldView-2 data. The average SOC values for each vegetation type were multiplied by their respective fraction images, and the resulting images were summed to produce total SOC estimates for the top 10 cm across the entire Ambolikha watershed according to both Landsat-5 and WorldView-2. The average SOC value for lake sediments was also included in the maps based on the isolated lakes. The maps provided both a spatial representation of SOC and numeric values (in g C m^{-2}) for the estimated quantity of C across the watershed. Finally, difference images were created by subtracting Landsat-5 fraction images from their respective WorldView-2 fraction images to indicate levels of agreement and disagreement for the classifications across space. If a pixel value in the difference image was positive, it corresponded to a higher pixel value (or estimated percentage of the land cover type) in the Landsat-5 fraction image (and vice versa). A difference image was produced in a similar manner for the total SOC quantity images for the top 10 cm of the soil column.

The area of each cover type and the total amount of SOC in the top 10 cm were also calculated based on the Landsat-5 and WorldView-2 classifications (both with and without SMA) to determine whether using SMA improved quantity estimations. These calculations involved multiplying the total area of each cover type by the average g C m^{-2} for each respective class for each method. When SMA was used, areas were calculated as the percentage of each pixel constituting each land cover type. Comparisons were made regarding the similarities and differences in the quantity and allocation of both the land cover types and total SOC values resulting from the data, classification method, and use of SMA.

A final hybrid map was produced combining individual land cover classes that were most accurate in the Landsat-5 and WorldView-2 classification maps according to the confusion matrices (e.g., alases were mapped more accurately under WorldView-2, so these areas became alases in the hybrid map). The individual SOC fraction images for each data type were also integrated, depending on which class was more accurately mapped, to create new estimates of SOC quantity and allocation in the top 10 cm. These hybrid maps offer a method for deriving estimates for SOC by utilizing the strengths of both Landsat-5 and WorldView-2.

4. Results

4.1. Field results

As measured in the field, the average organic layer depths for each vegetation type were 9.8 cm (±0.7 SE) for larch, 6.8 cm (±0.1 SE) for shrub, 16.4 cm (±1.6 SE) for floodplain, and 11.2 cm (±0.5 SE) for alas. The average soil C content (in g C m^{-2}) and SE for each vegetation type and lakes for the top 10 cm based on LOI calculations is shown in Table 2. Since the average organic layer depth for larch and shrub was less than 10 cm, the SOC values include a portion of the mineral soil to extend measurements to the top 10 cm of the soil column. Within this depth profile, shrubs contained the highest amount of SOC while floodplains had the least.

4.2. Land cover classification

The land cover classification outputs for the Landsat-5 imagery (using the Max Like classification) and the WorldView-2 imagery (using object-based classification) predict the spatial allocation of six land cover types (bare soil, water, larch, floodplain, shrub, and alas) (Figure 3a and b). The difference between the two classification outputs shows blue areas indicating agreement and black areas indicating disagreement (Figure 3c). Table 3 shows the number of pixels that agreed for each land cover as well as to which category pixels were allocated when they did not agree, with 67% overall agreement between the Landsat-5 and WorldView-2 maps. Based on the independent validation sites derived from the WorldView-2 image, the Landsat-5 map overall accuracy was 69%, with an average omission error of 31% and an average commission error of 29% (Table 4). The WorldView-2 map overall accuracy was 81%, with an average omission error of 19% and an average commission error of 18% (Table 5). In both the Landsat-5 and WorldView-2 classifications, shrub locations were overestimated (i.e., the commission error for shrub was greater than the omission error), while bare soil, floodplain, and alas were underestimated. The larch land cover class was slightly underestimated by Landsat-5 but

Table 2. Field measurements of organic layer depth and SOC content for the top 10 cm of soil by land cover type.

Cover type (*n*)	Organic layer depth (cm)	SOC for top 10 cm (g C m^{-2})
Alas (3)	11.2 (0.5)	4091.1 (885.1)
Floodplain (6)	16.4 (1.6)	3507.9 (721.0)
Lake (5)	NA	1525.6 (53.0)
Larch (19)	9.8 (0.7)	3510.3 (926.3)
Shrub (2)	6.8 (0.1)	7667.5 (2956.6)

Note: Values are means (±1 SE).
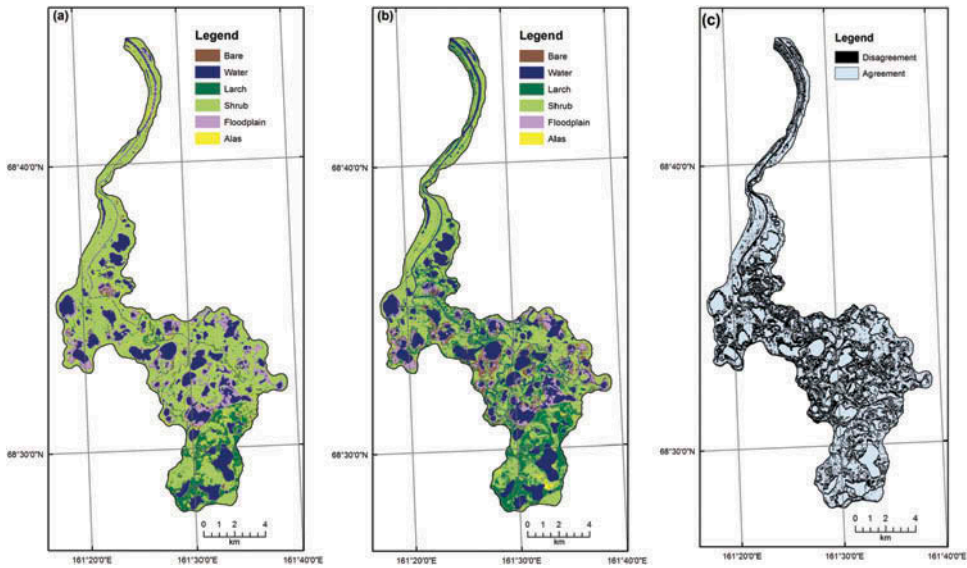
Figure 3. (a) Landsat-5 and (b) WorldView2 land-cover classifications for the Ambolikha River watershed showing bare soil, water, larch forest, shrub, floodplain, and alas with (c) agreement/ disagreement image.

overestimated by WorldView-2. The alas land cover class had the highest omission error in both classifications (49% in Landsat-5 and 29% in WorldView-2), whereas shrub had the largest commission error (49% in Landsat-5 and 33% in WorldView-2).

4.3. Soil C estimates

SMA produced fraction images for each vegetation type using the Landsat-5 and WorldView-2 classifications (Figure 4). The residual images had mean values of 0.073 for Landsat-5 and 0.023 for WorldView-2. Difference maps (Figure 4c, f, i, and l) display the spatial allocation of differences between the fraction images, with positive values (in red) representing higher fractions in the Landsat-5 image as compared with the WorldView-2 image. The average pixel values for each difference map were as follows: −0.002 for alas, −0.007 for floodplain, 0.015 for larch, and 0.008 for shrub, indicating that WorldView-2 predicted a higher percentage of alas and floodplain than Landsat-5. Histograms were produced for each fraction image to show the number of pixels classified as a percentage of alas, floodplain, larch, and shrub classes for Landsat-5 and WorldView-2 (Figure 5). The Landsat-5 trends are relatively noisy, while the WorldView-2 trends are significantly smoother.

Figure 6a and b illustrate the distribution and quantity of SOC in the top 10 cm and were created by multiplying the SMA fraction images by the corresponding SOC values for each vegetation type and applying the average lake SOC value to isolated water bodies. A difference map was produced to show the disagreement in the quantity and allocation of SOC estimated under each sensor (Figures 6c). Table 6 shows the average SOC (g C m^{-2}), area (km^2), and total SOC (Gg) for each land cover type and classification method, which were calculated using the areal estimates of each land cover type for the different classifications and the average field-based SOC values for each land cover type.

Table 3. Confusion matrix for pixel agreement between the Landsat-5 and WorldView-2 classification maps.

		WorldView-2 map							User's accuracy (%)	Commission error (%)
		Bare	Water	Larch	Shrub	Floodplain	Alas	Total		
Landsat-5 map	Bare	213.1	236.0	101.8	190.9	238.1	31.4	1011.2	21	79
	Water	4.6	4818.7	18.9	33.8	37.5	0.2	4913.7	98	2
	Larch	57.7	259.4	2125.3	545.4	28.4	7.6	3023.1	70	30
	Shrub	1076.7	214.4	2368.7	10,337.7	266.7	153.7	14,417.8	72	28
	Floodplain	215.5	1164.0	163.6	219.7	1261.4	2.8	3027.0	42	58
	Alas	9.4	66.6	721.0	646.8	4.8	8.7	1457.4	1	99
Total		1576.3	6759.1	5499.4	11,974.2	1837.0	204.4	27,850.4		
Producer's accuracy (%)		14	71	39	86	69	4			
Omission error (%)		86	29	61	14	31	96			

Note: Pixel counts are 1×10^3.

Table 4. Confusion matrix for the Landsat-5 classification and WorldView-2 validation data.

		WorldView-2 validation data							User's accuracy (%)	Commission error (%)
		Bare	Water	Larch	Shrub	Floodplain	Alas	Total		
Landsat-5 map	Bare	91	1	1	2	15	15	125	73	27
	Water	4	119	0	4	6	0	133	89	11
	Larch	2	6	112	5	9	9	143	78	22
	Shrub	25	5	23	126	25	42	246	51	49
	Floodplain	23	14	1	6	94	8	146	64	36
	Alas	5	5	13	7	1	76	107	71	29
Total		150	150	150	150	150	150	900		
Producer's accuracy (%)		61	79	75	84	63	51			
Omission error (%)		39	21	25	16	37	49			

Table 5. Confusion matrix for the WorldView-2 classification and WorldView-2 validation data.

		WorldView-2 validation data							
		Bare	Water	Larch	Shrub	Floodplain	Alas	Total	User's accuracy (%)	Commission error (%)
WorldView-2 classification	Bare	112	0	0	9	11	13	145	77	23
	Water	6	140	0	3	2	0	151	93	7
	Larch	4	0	138	20	12	11	185	75	25
	Shrub	11	5	12	116	12	18	174	67	33
	Floodplain	12	4	0	2	113	1	132	86	14
	Alas	5	1	0	0	0	107	113	95	5
Total		150	150	150	150	150	150	900		
Producer's accuracy (%)		75	93	92	77	75	71			
Omission error (%)		25	7	8	23	25	29			
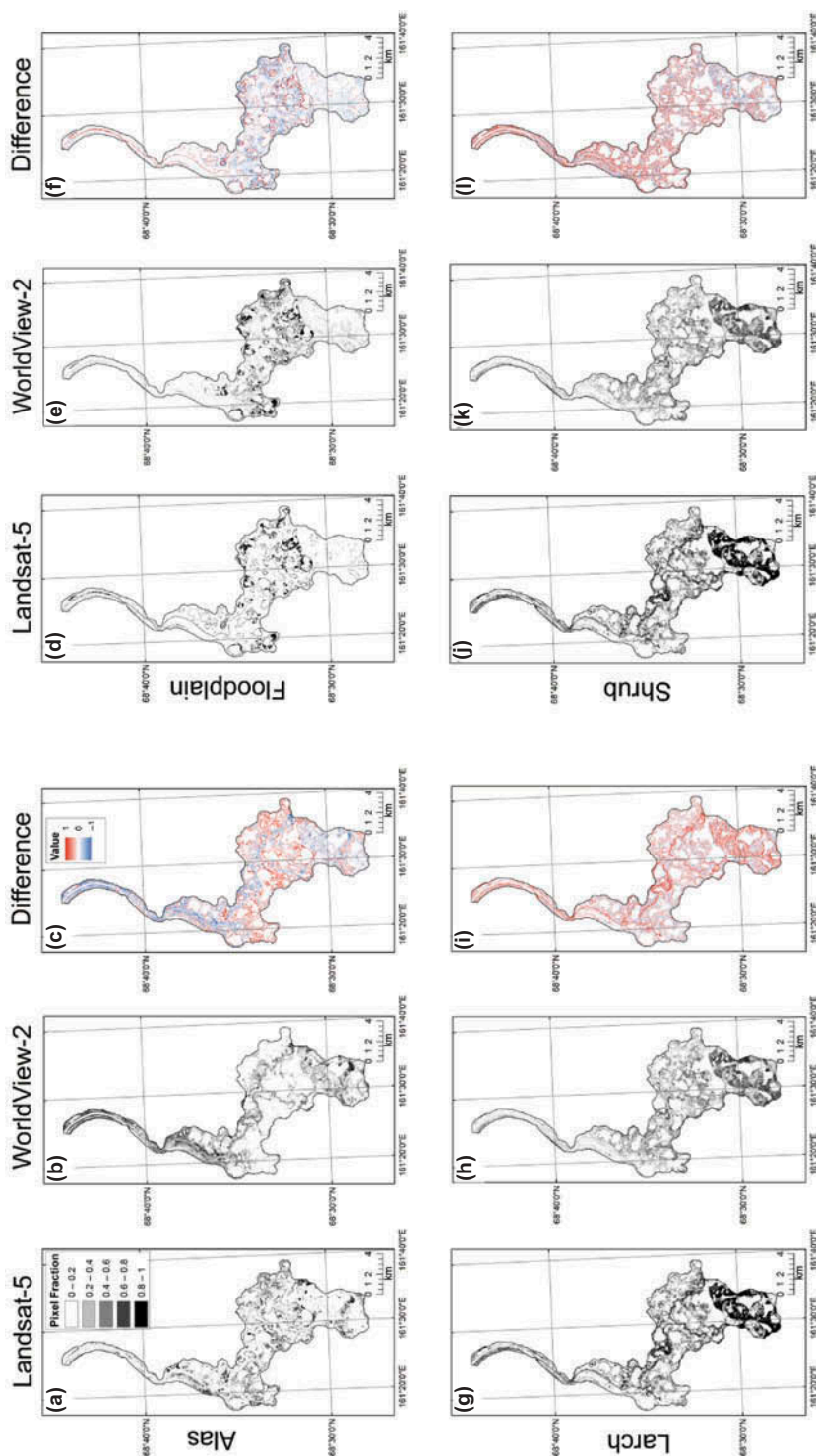
Figure 4. SMA fraction images for (a, d, g, j) Landsat-5 and (b, e, h, k) WorldView-2 by vegetation cover type and (c, f, i, l) difference images (where positive values indicate higher quantities estimated in the Landsat-5 map).
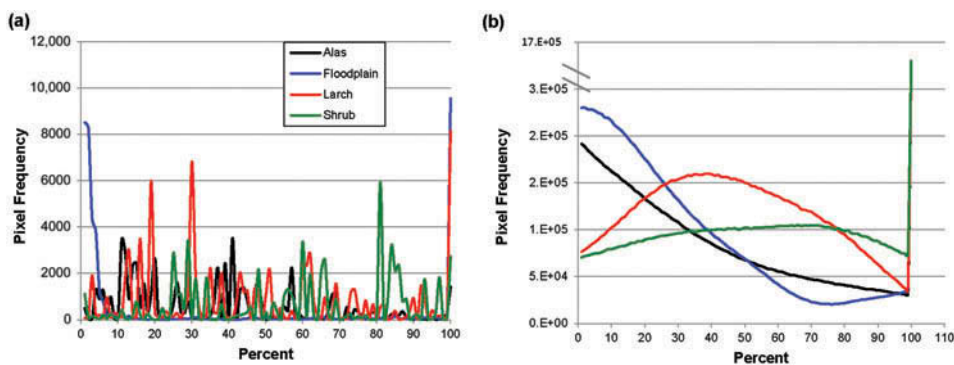
Figure 5. Histograms indicating the frequency of pixels classified as varying percentages of each vegetation type for SMA fraction images using (a) Landsat-5 and (b) WorldView-2.
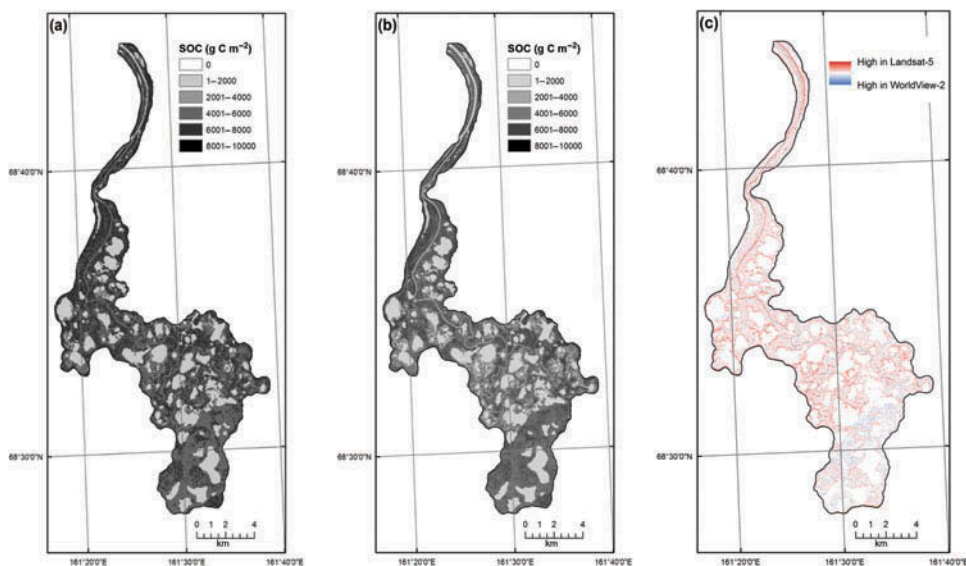
Figure 6. Top 10 cm SOC maps for the Ambolikha River watershed based on (a) Landsat-5 and (b) WorldView-2, with (c) difference image (where positive values indicate higher quantities estimated in Landsat-5 map).

The categories with the largest differences in area between the two classifications were larch and shrub, where the overall larch area was approximately 11 km^2 (~54%) smaller in the Landsat-5 map than in the WorldView-2 map. In contrast, the shrub area was approximately 30 km^2 (~53%) larger in the Landsat-5 map than in the WorldView-2 map.

Land cover-specific values were also summed to yield SOC estimates for the entire Ambolikha watershed. Within the top 10 cm (which also included SOC values for lakes), Landsat-5 estimated 633.4 Gg (without SMA) and 528.1 Gg (with SMA), whereas WorldView-2 estimated 557.3 Gg (without SMA) and 473.3 Gg (with SMA). There are also several notable results regarding the use of SMA to calculate areas for each vegetation class (Table 6). Using Landsat-5, the area of shrub decreased by 29 km^2 when SMA

Table 6. Average SOC (g m^2), area (km^2), and total SOC (Gg) for the Ambolikha River watershed based on classification and with or without use of SMA (total values for comparisons are italicized).

	Top 10 cm (g C m^{-2})	Area (km^2)	Top 10 cm total SOC (Gg)
Landsat-5 (no SMA)			
Larch	3510.3	13.1	46.0
Shrub	7667.5	63.1	483.8
Floodplain	3507.9	13.1	46.0
Alas	4091.1	6.4	26.2
Lake	1525.6	20.6	31.4
Total	–	*116.3*	*633.4*
Landsat-5 (SMA)			
Larch	3510.3	35.2	123.6
Shrub	7667.5	33.7	258.4
Floodplain	3507.9	11.6	40.7
Alas	4091.1	18.1	74.0
Lake	1525.6	20.6	31.4
Total	–	*119.3*	*528.1*
WorldView-2 (no SMA)			
Larch	3510.3	24.1	84.6
Shrub	7667.5	52.4	401.7
Floodplain	3507.9	7.9	27.7
Alas	4091.1	1.0	4.1
Lake	1525.6	25.7	39.2
Total	–	*111.0*	*557.3*
WorldView-2 (SMA)			
Larch	3510.3	23.5	82.5
Shrub	7667.5	27.5	210.9
Floodplain	3507.9	16.8	58.9
Alas	4091.1	20.0	81.8
Lake	1525.6	25.7	39.2
Total	–	*113.5*	*473.3*
Hybrid map (no SMA)			
Larch	3510.3	24.1	84.6
Shrub	7667.5	55.8	427.8
Floodplain	3507.9	7.9	27.7
Alas	4091.1	1.0	4.1
Lake	1525.6	25.7	39.2
Total	–	*114.5*	*583.4*
Hybrid map (SMA)			
Larch	3510.3	22.3	78.2
Shrub	7667.5	28.7	220.1
Floodplain	3507.9	18.9	66.3
Alas	4091.1	21.2	86.7
Lake	1525.6	25.7	39.2
Total	–	*116.8*	*490.5*

was utilized. In contrast, the larch area increased by 22 km^2 and the alas area increased by 12 km^2. Similarly, using WorldView-2 the area of shrub decreased by 25 km^2 when SMA was used, whereas floodplain and alas areas saw increases of 9 km^2 and 19 km^2, respectively. Finally, there were variable differences in areal estimates for certain vegetation types with regard to the classification method used. When SMA was not used, Landsat-5 estimated 13 km^2 of larch and WorldView-2 estimated 24 km^2, showing a
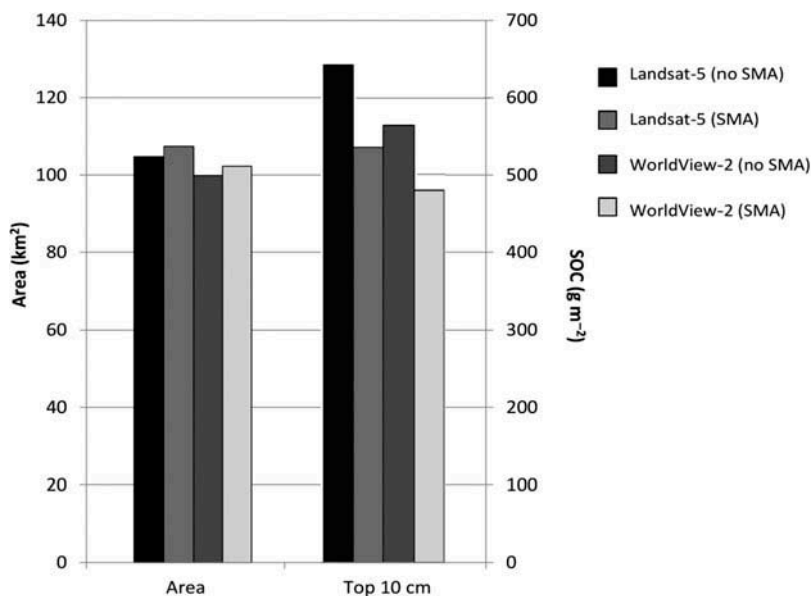
Figure 7.   Comparison showing area and top 10 cm SOC by classification method and use of SMA for the Ambolikha River watershed.

relatively large difference. However, when SMA was used, Landsat-5 predicted 18 km^2 for alas whereas WorldView-2 predicted 20 km^2. The data in Table 6 were summarized to display the total area and top 10 cm SOC for the Landsat-5 and WorldView-2 outputs, both with and without SMA (Figure 7).

The hybrid map involved identifying which sensor was more accurate on a per-class basis according to the confusion matrices (Figure 8). In particular, WorldView-2 had a higher accuracy for all classes except shrub, which was more accurately mapped by Landsat-5 (and the hybrid classes were assigned as such). Areas not classified as any of these categories (approximately 8 km^2) were compared visually with the WorldView-2 validation image to determine how the area should be classified, and were most commonly awarded to the shrub class. SOC quantities for the hybrid map within the top 10 cm estimates were 583.4 Gg without SMA and 490.5 Gg with SMA (Table 6). The overall accuracy of the hybrid classification map was 82%, with an average omission error of 18% and an average commission error of 17%.

5.   Discussion and conclusions

Based on these analyses, we report that the most predictable (non-hybrid) method for estimating SOC in the Ambolikha watershed comes from the fine spatial resolution WorldView-2 imagery, an object-based classification algorithm, and the use of SMA, estimating approximately 473.3 Gg in the top 10 cm (Figure 6b; Table 6). Object-based segmentation classification, based on WorldView-2 data with fine spatial resolution (1.85 m), was more accurate at mapping the land cover (81% overall accuracy, 18% average omission error, and 19% commission error) than a pixel-based Max Like classifier using medium spatial resolution (30 m) Landsat-5 data (69% overall accuracy, 29% average omission error, and 31% average commission error), with the majority of
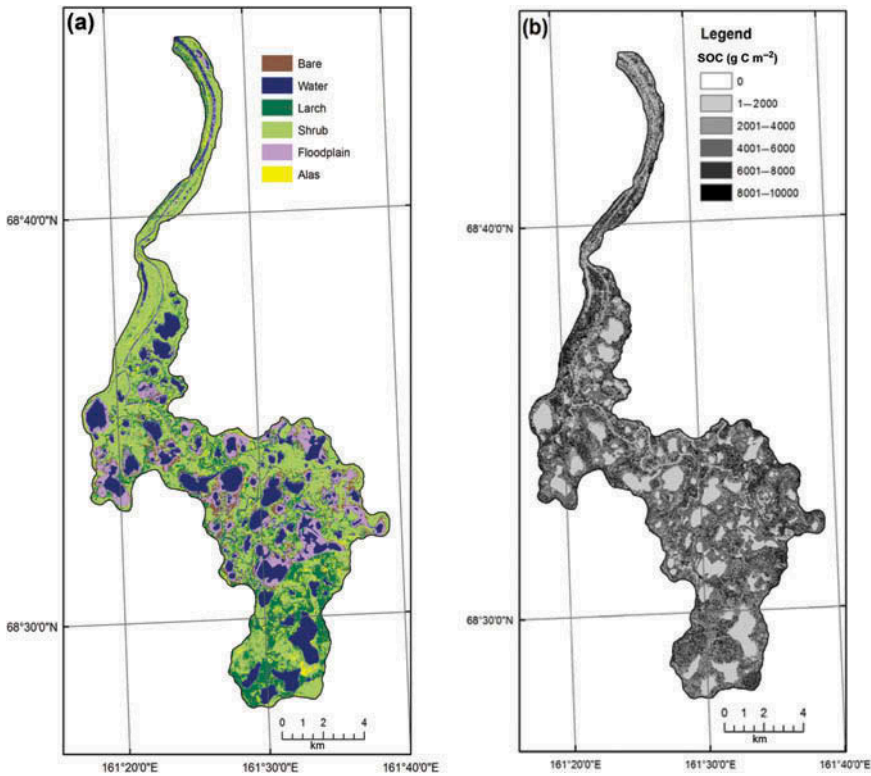
Figure 8.   (a) Hybrid classification map for the Ambolikha River watershed and (b) SOC for top 10 cm based on classes with highest accuracy for Landsat-5 and WorldView-2 classification.

disagreement between classifications involving the shrub and larch classes (Tables 3–5; Figure 3). Additionally, when compared with individual pixel values in the SOC maps where field data were collected, Landsat-5 overestimated the SOC quantity in the top 10 cm by 8%, WorldView-2 underestimated by 3%, and the hybrid overestimated by 1%.

The total amount of SOC varied depending on the classification method and use of SMA. For example, the difference between the highest and lowest SOC estimates was 167.9 Gg (without lakes, or 160.1 Gg including lakes). The WorldView-2 classification was deemed more accurate according to the validation data (Tables 3 and 4); however, even within WorldView-2, the use of SMA produced estimates that differed by 84.0 Gg. We determined that the use of SMA yields more accurate results because it can incorporate sub-pixel composition and associated SOC quantities for the top 10 cm. In a landscape where the majority of pixels are mixed, the use of SMA indeed produces a more precise estimate than would result from a hard classification even at fine spatial scales. SMA created a more realistic portrayal of SOC through a soft classification that involved multiple cover types within the same pixel. Given the nature of land cover types and distribution, this method is more representative than the one designating pixels as strictly one cover type in particular.

Previous studies comparing the use of high and medium resolution imagery for land cover classification routines have produced similar conclusions regarding map accuracy. In an exploratory study in China, Zhang and Zhu (2011) determined that the combination

of high-resolution QuickBird imagery and object-based classification incorporating texture resulted in a more accurate map than a pixel-based map based on spectral properties alone. Similarly, Hese, Grosse, and Pöcking (2010) determined that RapidEye data (spatial resolution of 6.5 m) had a higher classification accuracy than Landsat MSS data (spatial resolution of 80 m) when mapping changes in the lake area in the Lena River delta. In particular, small lakes and land-water boundaries were more accurately classified when a finer resolution and an object-based approach were employed. Fine spatial resolution imagery is particularly advantageous in areas where the cover type tends to vary rapidly because it can detect subtle changes that may be masked out at coarser spatial resolutions (e.g., Figure 5).

The histograms created for the SMA fraction images, showing the number of pixels classified as a percentage of each vegetation type, revealed noisy trends for the Landsat-5 images and smoother trends for WorldView-2 (Figure 5). These distributions justify the use of SMA for Landsat-5, revealing that the Landsat-5 pixels were consistently mixed owing to their coarser spatial resolution whereas the finer resolution of WorldView-2 resulted in fewer mixed pixels. Additionally, SMA helped reduce the inherent bias of the Max Like algorithm toward larger classes (i.e., classes with a higher probability of pixel membership) in the Landsat-5 classification, which likely explains why the area for shrub was almost twice as large when SMA was not used than when SMA was used. Finally, under SMA the omission and commission errors for most classes were greater than 25% for both the Landsat-5 and WorldView-2 classifications, suggesting that pixels could not be easily assigned to a single class because they had spectral characteristics of multiple classes (i.e., they contained a mixture of cover types). These findings support the use of SMA for rural landscape applications while expanding on previous studies describing the use of SMA to improve urban land cover classifications in mixed feature areas (Lu and Weng 2013; Tang and Pannelli 2009).

The SOC estimates for the top 10 cm in this study tend to be consistent with previous studies regarding relative quantities associated with different cover types. In terms of shrub and larch areas, which are made of the majority of the landscape in both classifications, higher SOC values for shrub are likely attributed to differences in above and belowground allocation of C (Jackson et al. 1996). Larch forests often have relatively higher aboveground C allocation, whereas shrubs tend to have deeper root profiles and therefore higher belowground allocation. In a study on the relationship between SOC, vegetation type, and climate, Jobbágy and Jackson (2000) reported similar conclusions, suggesting that the vegetation type had a stronger influence on SOC than direct effects of precipitation and temperature. As such, the land cover type has an important contribution to SOC quantities and can therefore be used as a robust proxy measurement when combining remote sensing with soil C estimates. However, as seen in the SE values for the SOC quantities, there also tends to be high variability within the same cover type, which may be attributed to the selection of sample sites to encompass variability and to be representative of landscape heterogeneity.

The total SOC quantities for the Ambolikha watershed also tend to be consistent with, but more locally specific than, previous studies quantifying Arctic SOC. In a northern circumpolar assessment of soil C, Hugelius et al. (2013) estimated 2500 to 5000 g C m^{-2} in the top 10 cm for the region (including the Ambolikha watershed). Our maps for the top 10 cm show the majority of values between 4000 and 7500 g C m^{-2}, suggesting that the Hugelius et al. (2013) assessment, designed as a global dataset, may underestimate SOC when used in localized applications owing to a coarser spatial resolution of data collection and extrapolation. Although SOC tends to be highly variable, even within the same land

cover types, our findings will likely help to improve this larger regional map by offering more precise estimations of SOC for specific areas (and for providing tested and improved satellite-based methodologies for doing so).

While the active layer thickness is not fully maximized until September (Frauenfeld et al. 2004), examining the organic layer is informative because considerable below-ground C is stored in this layer, despite its relatively shallow depth compared to perma-frost (Hinkel et al. 2003). We were limited to active layer organic rather than the entire organic layer because in lowland areas (floodplains, alases, and presumably lakes), the total organic layer extended into the permafrost and the full depth was not measured. However, our estimates of active layer organic SOC suggest that while floodplains comprise a small area of the watershed, they contain the greatest amount of SOC relative to other classes owing to a deep organic layer (and a shallow organic layer for larch and shrub areas; Table 2). In the top 10 cm alone, floodplains had the smallest amount of SOC relative to other vegetation classes. However, owing to the vertical distribution of SOC and the associated differences in SOC quantities for each cover type, when the entire organic layer is examined floodplains contain the greatest amount of SOC relative to the other classes. Wet, lowland areas tend to have higher SOC content than shrub or larch areas in the organic layer owing to an accumulation and concentration of dissolved organic carbon (DOC) in the soil as it leaches through vegetation on the ground and is transported by water from higher elevations (Schlesinger 1984). In addition, wet condi-tions of these low-lying areas create an anaerobic environment that further slows the rate of decomposition while increasing the buildup of SOC (Davidson and Janssens 2006). Ping et al. (2008) found that SOC in lowland areas of the North American Arctic was up to 18 times greater than in mountain soils.

Our measurements also allowed us to calculate SOC for the organic layer within the active layer for July. For active layer organic SOC, Landsat-5 estimated 476.4 Gg (without SMA) and 445.3 Gg (with SMA), WorldView-2 estimated 404.3 Gg (without SMA) and 411.3 (with SMA), and the hybrid map estimated 421.9 Gg without SMA and 431.0 Gg with SMA. In terms of the SMA calculations, Landsat-5 overestimated by 5%, WorldView-2 underestimated by 3%, and the hybrid map underestimated by 2%. Overall these values reflect a snapshot of SOC values in July rather than at maximum active layer thickness (occurring at the end of summer), therefore they likely underestimate total active layer SOC. However, these findings further support a finer spatial resolution and the use of SMA for land cover classification and calculations of SOC, as well as the integration of both datasets to produce the most accurate SOC estimate.

The data and methods used to produce the classification maps and SOC estimates impacted the results in several ways. A finer spatial resolution was able to better capture the heterogeneity of the landscape and use an object-oriented approach to classify clusters of pixels. Both classifications underestimated bare soil, floodplain, and alas areas, while overestimating shrubs. The Landsat-5 classification only underestimated floodplain areas by 1%, compared to 11% for WorldView-2, which may be attributed to the bands used by both classifications. The Landsat-5 classification included the visible, near-infrared (NIR), and short-wave infrared (SWIR) bands, while the WorldView-2 classification included only the visible and NIR bands. The sensitivity of SWIR to soil and vegetation moisture may explain why wet floodplains had a relatively low underestimation in the Landsat-5 map.

The hybrid classification and SOC quantity maps were produced to overcome the limitations of individual sensors and produce a more accurate map combining the strengths of both Landsat-5 and WorldView-2 (Table 6; Figure 8). The SOC quantity

for the top 10 cm is still overestimated (by 1%) when compared to SOC values from individual field sites, but the degree of overestimation is less than that of Landsat-5 or WorldView-2 alone. The degree of over or underestimation is based on individual pixel values from locations where samples were collected, yet not all sites were used because a portion of them fell outside of the study area and did not have a value in the SOC maps. Consequently, the percent of over or underestimation is based on a limited number of sites and serves only as an approximation for the rest of the map. However, the hybrid classification map still has the highest overall classification accuracy and the SOC maps have quantities closest to the field samples, justifying the use of the hybrid over individual sensors alone. The hybrid map provides a preliminary method for data fusion techniques that take advantage of the spatial resolution of WorldView-2 and the spectral resolution of Landsat-5 to produce the best classification method and subsequent estimations of SOC. By improving the classification accuracy of individual classes that performed best under each sensor, the overall accuracy of the hybrid map and SOC estimates may indeed continue to improve overestimates based on a single sensor. In this study, the hybrid map accuracy is only 1% higher than that of the WorldView-2 map, which can be attributed to the fact that it only incorporates one land cover class from the Landsat-5 map; however, in studies combining a similar number of classes from each sensor (e.g., three classes from WorldView-2 and three classes from Landsat-5), the advantages of a hybrid map would further increase.

The remote nature of our study location limited our overall sampling regime, but increasing the number of field sites for each cover type (particularly the shrub and alas classes) in future studies would help improve and strengthen the findings of this work. The broad characterization of the land cover type, chosen to correspond to our field data, could be further refined and stratified to include stand density and age in larch areas, fire history, elevation, and shrub genera, all of which may impact SOC. Our sampling sites were selected to be representative of the variability of each land cover type, but the consistent variation in SOC quantities (expressed through the SE) suggests that the stratification of cover types used here potentially mask meaningful trends. Additionally, obtaining measurements of the total organic layer depth (when it extends below the active layer) would allow extrapolations of SOC within the entire organic layer, adding another meaningful depth profile to this study. These full organic layer profiles would likely expose patterns and SOC estimates less evident in the top 10 cm alone, as seen with the high SOC values in floodplains when examining the active layer organic material in this land cover class.

We further acknowledge the inability of optical remote sensing to directly observe soil carbon and the associated limitation in deriving spatially extrapolated SOC estimates. Aboveground biophysical proxy measurements, including land cover and vegetation types, are commonly employed to address this issue (Jones, Guch, and Vonder Haar 1998; Gould 2000; Done and Wooldridge 2004; Gibbs et al. 2007; Rocchini et al. 2014). While vegetation biogeochemistry is a larger determinant of SOC lability and decomposition rate than temperature and moisture at the local scale, there may be meteorological variables influencing SOC, which are unaccounted for in this study (Jobbágy and Jackson 2000; Raich and Tufekciogul 2000; Shi et al. 2014). Despite these limitations, we have provided a preliminary assessment of how different remotely sensed data and classification methods can impact map accuracy and the estimated SOC values that result from such maps. We have also indicated that Landsat-5 overestimates SOC values more severely than WorldView-2 for both the top 10 cm and active layer organic; therefore, we find here that satellite data with a finer spatial resolution are optimal when mapping SOC at the landscape

scale. Finally, we have suggested a way to overcome the limitations of individual sensors by fusing data types to maximize the strengths of each.

The findings in this study are instructive for future work estimating SOC quantities in similar landscapes. Satellite data with a high spatial resolution, coupled with object-based classification and SMA, should be used when available to distinguish cover types and derive SOC estimates to extrapolate point-based field measurements across larger areas of the Arctic. As demonstrated, the coarser resolution of Landsat-5 resulted in an 8% over-estimation of SOC, compared with a 3% underestimation by WorldView-2. Additionally, integrating multiple sensors is useful in maximizing the strengths of different satellite data to detect land cover and estimate SOC in heterogeneous Arctic landscapes, as seen with the improved classification accuracy and SOC estimation (reduced to 1% overestimation) under the hybrid map. Finally, our results regarding SOC quantities contribute to existing estimates of SOC across the Arctic and provide precise numeric estimates on a regional scale. The findings presented here provide multiple avenues for their future use, including combining them with aboveground C quantities in the area to provide comprehensive estimates of terrestrial C, comparing them with SOC stocks in other areas of the Arctic to assess differences in C quantities, and integrating them with studies focusing on the cycling of C between terrestrial, hydrologic, and atmospheric reservoirs.

References

Abaimov, A. P. 2010. "Geographical Distribution and Genetics of Siberian Larch Species." *Permafrost Ecosystems: Siberian Larch Forests* 209: 41–58. doi:10.1007/978-1-4020-9693-8_3.

Alexander, H. D., M. C. Mack, S. Goetz, M. M. Loranty, P. S. A. Beck, K. Earl, and S. Zimov. 2012. "Carbon Accumulation Patterns During Post-Fire Succession in Cajander Larch (Larix Cajanderi) Forest of Siberia." *Ecosystems* 15: 1065–1082. doi:10.1007/s10021-012-9567-6.

Anisimov, O. A., F. E. Nelson, and A. V. Pavlov. 1999. "Predictive Scenarios of Permafrost Development under Conditions of Global Climate Change in the XXI Century." *Earth Cryology* 3: 15–25.

Bartalev, S. A., A. S. Belward, D. V. Erchov, A. S. Isaev, E. Bartholomé, V. Gond, P. Vogt, et al. 2003. *The Land Cover Map for Northern Eurasia for the Year 2000*. GLC2000 Database, European Commission Joint Research Centre.

Berner, L. T., P. S. A. Beck, M. M. Loranty, H. D. Alexander, M. C. Mack, and S. J. Goetz. 2012. "Cajander Larch (*Larix Cajanderi*) Biomass Distribution, Fire Regime and Post-Fire Recovery in Northeastern Siberia." *Biogeosciences* 9: 3943–3959. doi:10.5194/bg-9-3943-2012.

Chavez, P. S. 1996. "Image-Based Atmospheric Corrections – Revisited and Improved." *Photogrammetric Engineering and Remote Sensing* 62: 1025–1036.

Corradi, C., O. Kolle, K. Walter, S. A. Zimov, and E. D. Schulze. 2005. "Carbon Dioxide and Methane Exchange of a North-East Siberian Tussock Tundra." *Global Change Biology* 11: 1910–1925.

Davidson, E. A., and I. A. Janssens. 2006. "Temperature Sensitivity of Soil Carbon Decomposition and Feedbacks to Climate Change." *Nature* 440: 165–173. doi:10.1038/nature04514.

Denfeld, B. A., K. E. Frey, W. V. Sobczak, P. J. Mann, and R. M. Holmes. 2013. "Summer CO_2 Evasion from Streams and Rivers in the Kolyma River Basin, North-East Siberia." *Polar Research* 32: 19704. http://dx.doi.org/10.3402/polar.v32i0.19704.

Done, T., and S. Wooldridge. 2004. "Learning to Predict Large-Scale Coral Bleaching from past Events: A Bayesian Approach Using Remotely Sensed Data, In-Situ Data, and Environmental Proxies." *Coral Reefs* 23: 96–108. doi:10.1007/s00338-003-0361-y.

Eastman, J. R. 2012a. *IDRISI Selva*. Worcester, MA: Clark University.

Eastman, J. R. 2012b. "Segmentation." *IDRISI Help System*. Accessed in IDRISI Selva May 10, 2013. Worcester, MA: Clark University.

Frauenfeld, O. W., T. Zhang, R. G. Barry, and D. Gilichinsky. 2004. "Interdecadal Changes in Seasonal Freeze and Thaw Depths in Russia." *Journal of Geophysical Research* 109: D05101. doi:10.1029/2003JD004245.

Frey, K. E., and L. C. Smith. 2005. "Amplified Carbon Release from Vast West Siberian Peatlands by 2100." *Geophysical Research Letters* 32: L0940. doi:10.1029/2004GL022025.

Fuchs, H., P. Magdon, C. Kleinn, and H. Flessa. 2009. "Estimating Aboveground Carbon in a Catchment of the Siberian Forest Tundra: Combining Satellite Imagery and Field Inventory." *Remote Sensing of Environment* 113: 518–531. doi:10.1016/j.rse.2008.07.017.

Furyaev, V. V., E. A. Vaganov, N. M. Tchebakova, and E. N. Valendik. 2001. "Effects of Fire and Climate on Successions and Structural Changes in the Siberian Boreal Forest." *European Journal of Forest Research* 2: 1–15.

GEFSOC. 2006. "Assessment of Soil Organic Carbon Stocks and Change at National Scale." In *Technical Report of the Global Environment Facility Co-Financed Project No.: GFL-2740-02-4381*, edited by E. Milne. Fort Collins: Natural Resource Ecology Laboratory, Colorado State University. http://www.nrel.colostate.edu/projects/gefsoc-uk/GEFSOC_Technical_Report_web.pdf

Gibbs, H. K., S. Brown, J. O. Niles, and J. A. Foley. 2007. "Monitoring and Estimating Tropical Forest Carbon Stocks: Making REDD a Reality." *Environmental Research Letters* 2: 045023. doi:10.1088/1748-9326/2/4/045023.

Giner, N. M., and J. Rogan. 2012. "A Comparison of Landsat Etm+ and High-Resolution Aerial Orthophotos to Map Urban/Suburban Forest Cover in Massachusetts, USA." *Remote Sensing Letters* 3: 667–676. doi:10.1080/01431161.2012.656767.

Gould, W. 2000. "Remote Sensing of Vegetation, Plant Species Richness, and Regional Biodiversity Hotspots." *Ecological Applications* 10: 1861–1870. doi:10.1890/1051-0761(2000)010[1861:RSOVPS]2.0.CO;2.

Grosse, G., J. Harden, M. Turetsky, A. D. McGuire, P. Camill, C. Tarnocai, S. Frolking, et al. 2011. "Vulnerability of High-Latitude Soil Organic Carbon in North America to Disturbance." *Journal of Geophysical Research* 116: G00K06. doi:10.1029/2010JG001507.

Gupta, R. K., D. Vijayan, T. S. Prasad, and P. M. BalaManikavelu. 2004. "Assessing Limits of Classification Accuracy Attainable through Maximum Likelihood Method in Remote Sensing." *Journal of Water, Environment and Pollution* 1: 99–108.

Heikkinen, J. E. P., T. Virtanen, J. T. Huttunen, V. Elsakov, and P. J. Martikainen. 2004. "Carbon Balance in East European Tundra." *Global Biogeochemical Cycles* 18: 1–14. doi:10.1029/2003GB002054.

Hese, S., G. Grosse, and S. Pöcking. 2010. "Object Based Thermokarst Lake Change Mapping as Part of the ESA Data User Element (DUE) Permafrost." In *GEOBIA 2010-Geographic Object-*

Based Image Analysis, Ghent University, Ghent, June 29–July 2, edited by E. A. Addink and F. M. B. Van Coillie, Vol. XXXVIII-4/C7, Archives ISSN No 1682-1777. ISPRS.

Hinkel, K., W. R. Eisner, J. G. Bockheim, F. E. Nelson, K. M. Peterson, and X. Dai. 2003. "Spatial Extent, Age, and Carbon Stocks in Drained Thaw Lake Basins on the Barrow Peninsula, Alaska." *Arctic, Antarctic, and Alpine Research* 35: 291–300. doi:10.1657/1523-0430(2003) 035[0291:SEAACS]2.0.CO;2.

Huang, C.-Y., G. P. Asner, R. E. Martin, N. N. Barger, and J. C. Neff. 2009. "Multiscale Analysis of Tree Cover and Aboveground Carbon Stocks in Pinyon-Juniper Woodlands." *Ecological Applications* 19: 668–681. doi:10.1890/07-2103.1.

Hugelius, G., P. Kuhry, C. Tarnocai, and T. Virtanen. 2010. "Soil Organic Carbon Pools in a Periglacial Landscape: A Case Study from the Central Canadian Arctic." *Permafrost and Periglacial Processes* 21: 16–29. doi:10.1002/ppp.677.

Hugelius, G., C. Tarnocai, G. Broll, J. G. Canadell, P. Kuhry, and D. K. Swanson. 2013. "The Northern Circumpolar Soil Carbon Database: Spatially Distributed Datasets of Soil Coverage and Soil Carbon Storage in the Northern Permafrost Regions." *Earth System Science Data* 5: 3–13. doi:10.5194/essd-5-3-2013.

Jackson, R. B., J. Canadell, J. R. Ehleringer, H. A. Mooney, O. E. Sala, and E. D. Schulze. 1996. "A Global Analysis of Root Distributions for Terrestrial Biomes." *Oecologia* 108: 389–411. doi:10.1007/BF00333714.

Jobbágy, E. G., and R. B. Jackson. 2000. "The Vertical Distribution of Soil Organic Carbon and Its Relation to Climate and Vegetation." *Ecological Applications* 10: 423–436. doi:10.1890/1051-0761(2000)010[0423:TVDOSO]2.0.CO;2.

Jones, A. S., I. C. Guch, and T. H. Vonder Haar. 1998. "Data Assimilation of Satellite-Derived Heating Rates as Proxy Surface Wetness Data into a Regional Atmospheric Mesoscale Model. Part II: A Case Study." *Monthly Weather Review* 126: 646–667. doi:10.1175/1520-0493(1998) 126<0646:DAOSDH>2.0.CO;2.

Kajimoto, T., Y. Matsuura, A. Osawa, A. P. Abaimov, O. A. Zyryanova, A. P. Isaev, D. P. Yefremov, S. Mori, and T. Koike. 2006. "Size-Mass Allometry and Biomass Allocation of Two Larch Species Growing on the Continuous Permafrost Region in Siberia." *Forest Ecology and Management* 222: 314–325. doi:10.1016/j.foreco.2005.10.031.

Koutaniemi, L. 1985. "The Central Yakutian Lowlands: Land of Climatic Extremes, Permafrost and Alas Depressions." *Soviet Geography* 26: 421–436.

Lu, D., and Q. Weng. 2013. "Spectral Mixture Analysis of the Urban Landscape in Indianapolis with Landsat ETM+ Imagery." *Photogrammetric Engineering & Remote Sensing* 70: 1053–1062. doi:10.14358/PERS.70.9.1053.

NCDC. 2012. "Global Summary of the Day." Station Cherskij. NNDC Climate Data Online: National Climate Data Center. Accessed March 14, 2013. http://www.ncdc.noaa.gov/oa/ climate/onlineprod/drought/xmgr.html

Oechel, W. C., and G. L. Vourlitis. 1994. "The Effects of Climate Charge on Land—Atmosphere Feedbacks in Arctic Tundra Regions." *Trends in Ecology and Evolution* 9: 324–329. doi:10.1016/0169-5347(94)90152-X.

Perea, A. J., J. E. Meroño, and M. J. Aguilera. 2009. "Algorithms of Expert Classification Applied in Quickbird Satellite Images for Land Use Mapping." *Chilean Journal of Agricultural Research* 69: 400–405. doi:10.4067/S0718-58392009000300013.

Ping, C.-L., G. J. Michaelson, M. T. Jorgenson, J. M. Kimble, H. Epstein, V. E. Romanovsky, and D. A. Walker. 2008. "High Stocks of Soil Organic Carbon in the North American Arctic Region." *Nature Geoscience* 1: 615–619. doi:10.1038/ngeo284.

Potter, C. 2014. "Regional Analysis of MODIS Satellite Greenness Trends for Ecosystems of Interior Alaska." *GIScience and Remote Sensing* 51: 390–402. doi:10.1080/ 15481603.2014.933606.

Raich, J. W., and A. Tufekciogul. 2000. "Vegetation and Soil Respiration: Correlations and Controls." *Biogeochemistry* 48: 71–90. doi:10.1023/A:1006112000616.

Reeuwijk, L. P. 2002. "Procedures for Soil Analysis." Technical Paper. Wageningen: International Soil Reference and Information Center.

Richards, J. A. 1986. *Remote Sensing Digital Image Analysis*. Berlin: Springer-Verlag.

Rocchini, D., L. Dadalt, L. Delucchi, M. Neteler, and M. W. Palmer. 2014. "Disentangling the Role of Remotely Sensed Spectral Heterogeneity as a Proxy for North American Plant Species Richness." *Community Ecology* 15: 37–43. doi:10.1556/ComEc.15.2014.1.4.

Rogan, J., and D. M. Chen. 2004. "Remote Sensing Technology for Mapping and Monitoring Land-Cover and Land-Use Change." *Progress in Planning* 61: 301–325. doi:10.1016/S0305-9006(03)00066-7.

Schepaschenko, D. G., A. Z. Shvidenko, and V. S. Shalaev. 2008. *Biological Productivity and Carbon Budget of Larch Forests of Northern-East Russia*, 296. [In Russian]. Moscow: Moscow State Forest University.

Schlesinger, W. H. 1984. "Chapter 4, Soil Organic Matter: A Source of Atmospheric CO_2." In *The Role of Terrestrial Vegetation in the Global Carbon Cycle: Measurement by Remote Sensing*, edited by G. M. Woodwell. New York: John Wiley and Sons Ltd.

Schuur, E. A. G., J. Bockheim, J. G. Canadell, E. Euskirchen, C. B. Field, S. V. Goryachkin, S. Hagemann, et al. 2008. "Vulnerability of Permafrost Carbon to Climate Change: Implications for the Global Carbon Cycle." *Bioscience* 58: 701–714. doi:10.1641/B580807.

Settle, J. J., and N. A. Drake. 1993. "Linear Mixing and the Estimation of Ground Cover Proportions." *International Journal of Remote Sensing* 14: 1159–1177. doi:10.1080/01431169308904402.

Shafri, H. Z. M., A. Suhaili, and S. Mansor. 2007. "The Performance of Maximum Likelihood, Spectral Angle Mapper, Neural Network and Decision Tree Classifiers in Hyperspectral Image Analysis." *Journal of Computer Science* 3: 419–423. doi:10.3844/jcssp.2007.419.423.

Shi, Y., X. Xiang, C. Shen, H. Chu, J. D. Neufeld, V. K. Walker, and P. Grogan 2014. "Vegetation-Associated Impacts on Arctic Tundra Bacterial and Micro-Eukaryotic Communities." *Applied Environmental Microbiology* 81: 492–501.

Sitch, S., A. D. McGuire, J. Kimball, N. Gedney, J. Gamon, R. Engstrom, A. Wolf, Q. Zhuang, J. Clein, and K. C. McDonald. 2007. "Assessing the Carbon Balance of Circumpolar Arctic Tundra Using Remote Sensing and Process Modeling." *Ecological Applications* 17: 213–234. doi:10.1890/1051-0761(2007)017[0213:ATCBOC]2.0.CO;2.

Sohn, Y., and R. M. McCoy. 1997. "Mapping Desert Shrub Rangeland Using Spectral Mixtures with TM Data." *Photogrammetric Engineering and Remote Sensing* 63: 707–716.

Stow, D. A., A. Hope, D. McGuire, D. Verbyla, J. Gamon, F. Huemmrich, S. Houston, et al. 2004. "Remote Sensing of Vegetation and Land Cover Change in Arctic Tundra Ecosystems." *Remote Sensing of Environment* 89: 281–308. doi:10.1016/j.rse.2003.10.018.

Szakacs, G. G. J., C. C. Cerri, U. Herpin, and M. Bernoux. 2011. "Assessing Soil Carbon Stocks under Pastures through Orbital Remote Sensing." *Scientia Agricola (Piracicaba, Brazil)* 68: 574–581.

Tang, Y., and C. W. Pannelli. 2009. "A Hybrid Approach for Land Use/Land Cover Classification." *GIScience and Remote Sensing* 46: 365–387. doi:10.2747/1548-1603.46.4.365.

Tank, S. E., K. E. Frey, R. G. Striegl, P. A. Raymond, R. M. Holmes, J. W. McClelland, and B. J. Peterson. 2012. "Landscape-Level Controls on Dissolved Carbon Flux from Diverse Catchments of the Circumboreal." *Global Biogeochemical Cycles* 26: GB0E02. doi:10.1029/2012GB004299.

Tarnocai, C., J. G. Canadell, E. A. G. Schuur, P. Kuhry, G. Mazhitova, and S. Zimov. 2009. "Soil Organic Carbon Pools in the Northern Circumpolar Permafrost Region." *Global Biogeochemical Cycles* 23: GB2023. doi:10.1029/2008GB003327.

Tarnocai, C., J. M. Kimble, D. Swanson, S. Goryachkin, Y. M. Naumov, V. Stolbovoi, B. Jakobsen, et al. 2002. *Northern Circumpolar Soils*. 1:10,000,000 Scale Map. Ottawa: Research Branch, Agriculture and Agri-Food Canada. Distributed by the National Snow and Ice Data Center, Boulder, CO.

Thomas, N., C. Hendrix, and R. G. Congalton. 2003. "A Comparison of Urban Mapping Methods Using High-Resolution Digital Imagery." *Photogrammetric Engineering and Remote Sensing* 69: 963–972. doi:10.14358/PERS.69.9.963.

Turner, D. P., S. V. Ollinger, and J. S. Kimball. 2004. "Integrating Remote Sensing and Ecosystem Process Models for Landscape to Regional Scale Analysis of the Carbon Cycle." *Bioscience* 54: 573–584. doi:10.1641/0006-3568(2004)054[0573:IRSAEP]2.0.CO;2.

Updike, T., and C. Comp. 2010. *Radiometric Use of Worldview-2 Imagery: Technical Note*. Longmont, CO: DigitalGlobe, Inc.

USGS. 2011. "Hydro 1K Asia." Earth Resources Observation and Science (EROS) Center. Accessed March 14, 2013. http://eros.usgs.gov/#/Find_Data/Products_and_Data_Available/gtopo30/hydro/asia

Walter, K., S. Zimov, J. Chanton, D. Verbyla, and F. Chapin III. 2006. "Methane Bubbling from Siberian Thaw Lakes as a Positive Feedback to Climate Warming." *Nature* 443: 71–75. 10.1038/nature05040

Wulder, M. A., R. J. Hall, N. C. Coops, and S. E. Franklin. 2004. "High Spatial Resolution Remotely Sensed Data for Ecosystem Characterization." *Bioscience* 54: 511–521. doi:10.1641/0006-3568(2004)054[0511:HSRRSD]2.0.CO;2.

Zhang, R., and D. Zhu. 2011. "Study of Land Cover Classification Based on Knowledge Rules Using High-Resolution Remote Sensing Images." *Expert Systems with Applications* 38: 3647–3652. doi:10.1016/j.eswa.2010.09.019.

Zhou, T., P. Shi, J. Luo, and Z. Shao. 2008. "Estimation of Soil Organic Carbon Based on Remote Sensing and Process Model." *Journal of Remote Sensing* 11: 139–147.

Zimov, S. A., S. P. Davydov, G. M. Zimova, A. I. Davydova, E. A. G. Schuur, K. Dutta, and F. S. Chapin. 2006. "Permafrost Carbon: Stock and Decomposability of a Globally Significant Carbon Pool." *Geophysical Research Letters* 33 III: L20502. 10.1029/2006GL027484